J. Fluid Mech. (1984), *vol.* 146, *pp.* 253–270
Printed in Great Britain

Self-consistent effective-medium parameters for oceanic internal waves

By R. J. DEWITT
Physics Department, Southern Arkansas University, Magnolia, Arkansas 71753
AND JON WRIGHT
Center for Studies of Nonlinear Dynamics, La Jolla Institute, 8950 Villa La Jolla Drive, Suite 2150, La Jolla, CA 92037

(Received 4 October 1982 and in revised form 18 April 1984)

In this paper we apply a formalism introduced in a previous paper to write down a self-consistent set of equations for the functions that describe the near-equilibrium time behaviour of random oceanic internal waves. These equations are based on the direct-interaction approximation. The self-consistent equations are solved numerically (using the Garrett–Munk spectrum as input) and the results are compared to parameters obtained in the weak-interaction approximation (WIA). The formalism points out that an extra parameter that is implicitly vanishingly small in the WIA has a significant effect on decay rates when computed self-consistently. We end by mentioning possible future self-consistent calculations that would improve upon our own.

1. Introduction

In the past few years the study of transfer of energy in the internal-wave field of the ocean has become an active area of research. Olbers (1976), McComas (1977), Pomphrey, Meiss & Watson (1980), and DeWitt & Wright (1982), have done calculations in the resonant-interaction approximation (RIA, also called weak-interaction approximation, WIA) of lifetimes and action transfer rates.

There has been a continuing controversy during the last few years regarding the validity of the RIA. In addition to the above references see also McComas & Muller (1981), Fredericksen & Bell (1983), Carnevale & Fredericksen (1983*a*) and Holloway (1980, 1982) for a further discussion of this point. The previous calculations implicitly assumed that the interactions were weak and that the lifetimes of modes were long compared to other relevant timescales. In our approach, the nature of this approximation will be made clearer. Intuitively, it is easy to understand one source of the short lifetime. Consider the interaction of an infinitesimal small-scale wave (test wave) with large-scale inertial waves. The interaction consists of advection by the large-scale waves and a rapid change in the wavenumber of the test wave, both in magnitude and direction (see Holloway 1979 and references therein). Attempts at solving this part of the problem have been made by Meiss & Watson (1982), Henyey & Pomphrey (1983) and Henyey, Pomphrey & Meiss (1983). In this paper we present a calculation using the formalism presented in DeWitt & Wright (1982) and DeWitt (1982). The idea is to use the direct-interaction approximation (DIA). In fact we will use additional approximations to the DIA. The details and further references can be found in DeWitt & Wright (1982) or DeWitt (1982).

The DIA equations give an effective linear theory with memory terms and forcing terms. The memory function and forcing function are determined by a self-consistent calculation that will be described in §2. In this section we write down the effective linear theory, as that will enable the reader to better understand what is being calculated.

Our formulation of the nonlinear problem is the same as that of McComas (1977) or Meiss, Pomphrey & Watson (1979). We review the equations very briefly. A Lagrangian is introduced with the variable being the displacement field $\xi_j(\boldsymbol{r}, t)$:

$$L(\xi) = \tfrac{1}{2}\rho(\dot{\xi}_j\dot{\xi}_j + e_{jkl}f_j\dot{\xi}_k\xi_1) - \rho g\xi_j\delta_{j3} - \left[\xi_j\frac{\partial P_e}{\partial r_j} + \tfrac{1}{2}\xi_j\xi_k\frac{\partial^2 P_e}{\partial r_j\partial r_k} + \ldots\right] - \left[\xi_j\frac{\partial \pi}{\partial r_j} + \tfrac{1}{2}\xi_j\xi_k\frac{\partial^2 \pi}{\partial r_j\partial r_j} + \ldots\right]. \quad (1.1)$$

ξ is then expanded in terms of the normal modes:

$$\xi_j(\boldsymbol{r}, t) = \sum_{s=\pm}\int \mathrm{d}^3k\, A_k^s(t)\, Z_{kj}^s\, \mathrm{e}^{\mathrm{i}\boldsymbol{k}\cdot\boldsymbol{r}}, \quad (1.2)$$

where $A^{\pm}(t)$ are the mode amplitudes for linear waves. The amplitude for waves with phase velocity along $\boldsymbol{k}$ is A^+, and the amplitude for waves with phase velocity in the negative $\boldsymbol{k}$-direction is A^-. The amplitudes satisfy the equations

$$\dot{A}_k^s(t) + \mathrm{i}\Omega_k^s(t) + \nu_0(k)\, A_k^s(t) + \sum_{1,2}\int \mathrm{d}^3\boldsymbol{k}_1\,\mathrm{d}^3\boldsymbol{k}_2\,\delta(\boldsymbol{k}-\boldsymbol{k}_1-\boldsymbol{k}_2) \times B_{k-k_1-k_2}^{s-s_1-s_2}\, A_{k_1}^{s_1} A_{k_2}^{s_2} = f_0^s(\boldsymbol{k}, t). \quad (1.3)$$

For details on the coefficients Z and the couplings B see DeWitt (1982), Olbers (1976) or Meiss *et al.* (1979). A term $\nu_0(k)$ has been added to simulate dissipation due to interaction with the environment. $f_0(k)$ simulates forcing from the environment, and Ω_k is the dispersion relation

$$\Omega_k = \left(\frac{N^2k_{\mathrm{h}}^2 + f^2k_{\mathrm{v}}^2}{k_{\mathrm{h}}^2 + k_{\mathrm{v}}^2}\right)^{\frac{1}{2}}.$$

In the DIA approximation all of the Green functions and correlation functions are identical with those of the following linear system of equations:

$$\left.\begin{aligned}\frac{\mathrm{d}A^-}{\mathrm{d}t}(\boldsymbol{k}, t) + \int_{-\infty}^{\infty}[\Gamma_{+-}(\boldsymbol{k}, t, t')\, A^-(\boldsymbol{k}, t') + \Gamma_{++}(\boldsymbol{k}, t, t')\, A^+(\boldsymbol{k}, t')]\,\mathrm{d}t' &= f^-(\boldsymbol{k}, t),\\ \frac{\mathrm{d}A^+}{\mathrm{d}t}(\boldsymbol{k}, t) + \int_{-\infty}^{\infty}[\Gamma_{--}(\boldsymbol{k}, t, t')\, A^-(\boldsymbol{k}, t') + \Gamma_{-+}(\boldsymbol{k}, t, t')\, A^+(\boldsymbol{k}, t')]\,\mathrm{d}t' &= f^+(\boldsymbol{k}, t).\end{aligned}\right\} \quad (1.4)$$

$\Gamma(t, t')$ is a function determined by the DIA equations. Causality demands $\Gamma(t, t') = 0$ for $t > t$. We are treating a stationary problem, so Γ depends only on $t - t'$. $f(\boldsymbol{k}, t)$ is a random forcing function on the kth mode due to all of the other modes and any external random forces. In the DIA approximation the fs are Gaussian random variables with zero mean (provided that the external forces are also Gaussian with zero mean). Their correlation function is given by

$$F_0(\boldsymbol{k}, t-t')\,\delta_{s,-s'} + \Sigma_2^{ss'}(\boldsymbol{k}, t-t') = \langle f^s(\boldsymbol{k}, t) f^{s'}(\boldsymbol{k}', t')\rangle. \quad (1.5)$$

F_0 is the correlation function for the external part of the forces and the matrix $\boldsymbol{\Sigma}_2$ is calculated from the DIA equations.

The DIA equations involve self-consistent equations for two-point correlation and

response functions. Although three- and four-point functions can be calculated, they are not determined self-consistently, and we have not calculated them. Two-point functions with different wave vectors would not necessarily vanish in a nonlinear system, but we are assuming homogeneity, so they will vanish by assumption. However, the amplitudes for travelling waves parallel and antiparallel to a wave vector $\boldsymbol{k}$ have the same wave vector, so that homogeneity does not force the vanishing of their two-point function. This is the origin of the terms Γ_{++} and Γ_{--}, which vanish for linear waves.

It is convenient to work with the Fourier transform in the time domain, where Γ has the following representation:

$$\Gamma^{ss'}(\boldsymbol{k},\omega) = \delta_{s,-s'}[\nu_0(\boldsymbol{k}) + \mathrm{i}\Omega^{-s}(\boldsymbol{k})] - \Sigma_1^{ss'}(\boldsymbol{k},\omega). \tag{1.6}$$

Here ν_0 is the damping due to interaction with the external environment and $\Omega^{\pm} = \pm\Omega_k$. If $\boldsymbol{\Sigma}_1$ were independent of ω it would represent three effects. The obvious ones are a finite lifetime and frequency shift. In addition, however, there is a coupling between the $\pm$ mode. The dependence of $\boldsymbol{\Sigma}_1$ on ω represents a contribution to $\mathrm{d}A/\mathrm{d}t$ from previous times; that is, there is a memory effect. Similarly the ω-dependence of $\boldsymbol{\Sigma}_2$ says that the effective force on one mode due to other modes cannot be white noise, and that the force at one time is correlated with the force at a different time.

Previous calculations have used weak-interaction theory, which is the limit of the DIA equation in which $\boldsymbol{\Sigma}_1$ and $\boldsymbol{\Sigma}_2$ are independent of ω and infinitesimal.

In a previous paper (DeWitt & Wright 1982) we examined the dependence of $\boldsymbol{\Sigma}_1$ and $\boldsymbol{\Sigma}_2$ on ω assuming that the RIA was valid. There we found that $\boldsymbol{\Sigma}_1$ and $\boldsymbol{\Sigma}_2$ had some ω-dependence in lowest-order perturbation theory. In this paper we will check the assumption of infinitesimal $\boldsymbol{\Sigma}_1$ and $\boldsymbol{\Sigma}_2$, ignoring, however, the ω-dependence. The reason for this is that the calculations were too difficult if ω dependence of the $\boldsymbol{\Sigma}$s was allowed. We expect that there would probably be some changes in our answers if we were able to do a more complete calculation.

In §2 we introduce the correlation function for the As,

$$\frac{1}{2\pi} U^{ss'}(\boldsymbol{k},\omega)\,\delta^3(\boldsymbol{k}+\boldsymbol{k})\,\delta(\omega+\omega') = \langle A_k^s(\omega)\,A_{k'}^{s'}(\omega')\rangle, \tag{1.7}$$

and the Green function for (1.3),

$$G^{ss'}(\boldsymbol{k},\omega) = [(\nu_0 + \mathrm{i}\Omega_k^{-s})\,\delta_{s,-s'} - \mathrm{i}\omega - \mathrm{i}\Sigma_1^{ss'}(\boldsymbol{k},\omega)]^{-1}. \tag{1.8}$$

The inverse is a matrix inverse of a 2×2 matrix.

To summarize, the DIA equations attempt an approximate calculation of the two-point functions, i.e. the response and correlation functions. All of the information is contained in two functions, $\boldsymbol{\Sigma}_1(\boldsymbol{k},\omega)$ and $\boldsymbol{\Sigma}_2(\boldsymbol{k},\omega)$. The direct-interaction approximation for $\boldsymbol{\Sigma}_1$ and $\boldsymbol{\Sigma}_2$ is a set of equations that determine them self-consistently. These equations are presented in §2. There are a number of questions that naturally arise about the equations. How valid are they? How does one assess the validity of any answers? How does one solve them? Are the solutions unique? Those are questions for which we have no clear answers. These equations are modelled after self-consistent equations for other systems that have been highly successful; for example Hartree calculations in atomic physics and mean-field calculations for fields in magnetic materials. In turbulence this approximation often gives good answers for low-to-moderate Reynolds numbers. Lacking simulations to compare with it is difficult to make an accurate assessment. In this regard see Fredericksen & Bell (1983).

The problem of actually solving the equations is very difficult. In fact we have been

forced to make additional approximations beyond DIA – principally that $\boldsymbol{\Sigma}_1$ and $\boldsymbol{\Sigma}_2$ are independent of ω. Although it is again difficult to justify this approximation, it has some virtues. One is that it allows us to assess the validity of previous calculations that used weak-interaction theory (WIA). The reason for this is that if WIA were valid our results would then reproduce WIA exactly as $\boldsymbol{\Sigma}_1$ and $\boldsymbol{\Sigma}_2$ would be infinitesimal. This ability to check WIA is a very important feature of this paper.

We find substantial differences from weak-interaction rates for many of the internal wave modes, since the functions $\boldsymbol{\Sigma}_1(\boldsymbol{k})$ and $\boldsymbol{\Sigma}_2(\boldsymbol{k})$ are quite different from those of weak interactions. One problem that immediately arises is that if $\boldsymbol{\Sigma}_1$ and $\boldsymbol{\Sigma}_2$ are large the validity of truncating the Lagrangian in (1.1) at third order is suspect. A Eulerian formulation would remove this problem. Carnevale & Frederickson (1983*a*) have discussed the 2-dimensional Eulerian DIA equations for internal waves and the relationship to WIA. They pointed out that WIA imposes a spurious conservation law. In this paper we use (1.1) and ignore higher-order corrections without attempting to justify that approximation.

The remainder of the paper is organized into four sections. In §2 we write down the DIA equations and our approximation to them. In §3 we discuss briefly the meaning of the parameters, and in §4 we give the results of our calculations. Section 5 gives our conclusions.

2. The self-consistent equations

In this section we write down the specific equations that will be used in the numerical solution of the problem. The derivation of the more general direct-interaction approximation (DIA) equations is given in DeWitt & Wright (1982). The exact DIA equations are

$$\Sigma_1^{ss'}(\boldsymbol{k},\omega) = \frac{2}{\pi} \sum_{\substack{s_1, s_1' \\ s_2, s_2'}} \int \mathrm{d}^3\boldsymbol{k}_1\, \mathrm{d}^3\boldsymbol{k}_2\, \mathrm{d}\omega_1\, \mathrm{d}\omega_2\, \delta(\boldsymbol{k}+\boldsymbol{k}_2-\boldsymbol{k}_1)\, \delta(\omega+\omega_2-\omega_1)\, B^{-ss_2-s_1}_{k k_2 -k_1} \times B^{-s_1 s_2 - s'}_{k_1 - k_2 - k} [iG^{s_1 s_1'}(\boldsymbol{k}_1,\omega_1)]\,[-U^{s_2 s_2'}(\boldsymbol{k}_2,\omega_2)] \quad (2.1)$$

and

$$\Sigma_2^{ss'}(\boldsymbol{k},\omega) = \frac{1}{\pi} \sum_{\substack{s_1, s_1' \\ s_2, s_2'}} \int \mathrm{d}^3\boldsymbol{k}_1\, \mathrm{d}^3\boldsymbol{k}_2\, \mathrm{d}\omega_1\, \mathrm{d}\omega_2\, \delta(\boldsymbol{k}+\boldsymbol{k}_2+\boldsymbol{k}_1)\, \delta(\omega+\omega_2+\omega_1)\, B^{-ss_1 s_2}_{k k_1 k_2} \times B^{-s s_1' s_2'}_{-k k_1 - k_2} U^{s_1 s_1'}(\boldsymbol{k}_1,\omega_1) U^{s_2 s_2'}(\boldsymbol{k}_2,\omega_2), \quad (2.2)$$

where G is given by (1.8) and U by

$$U^{ss'}(\boldsymbol{k},\omega) = \sum_{s_1, s_2} G^{ss_1}(\boldsymbol{k},\omega)\,[\delta_{s,-s'} F_0(\boldsymbol{k},\omega) + \Sigma_2^{s_1 s_2}(\boldsymbol{k},\omega)]\, G^{s's_2}(-\boldsymbol{k}_1-\omega). \quad (2.3)$$

The goal of the calculation is to compute the matrices $\boldsymbol{\Sigma}_1$ and $\boldsymbol{\Sigma}_2$ in a self-consistent manner. All of the information about the decay and correlation of the waves is contained in these two quantities.

As was pointed out in the previous paper, much has been said about possible ways to solve systems of equations that are related to the full DIA set of equations. However, the only numerical attempts at solution in this framework have used the RIA, which computes Σ_1^{-+} and Σ_2^{-+} by letting

$$\boldsymbol{\Sigma}_1, \boldsymbol{\Sigma}_2 \to 0 \quad (2.4)$$

in the expressions on the right-hand sides of (2.1) and (2.2). The only outcome that

would justify this approach would be one in which the computed values of $\boldsymbol{\Sigma}_1$ were small compared with typical timescales.

When there are many timescales present, it is not always clear what scales should be compared. In our approach we can compare the results from assuming $\boldsymbol{\Sigma}_1$ is infinitesimal with those from using its actual value.

Our parametrization of the DIA equations assumes that $G(\boldsymbol{k}, \omega)$ can be represented by two poles, one at $\omega = \Omega_r - i\alpha_I$ and a second at $\omega = -\Omega_r - ia_I$. Symmetry between $\pm\boldsymbol{k}$ is assumed as well as between $\pm\Omega$. The equations are then parametrized by the pole positions. Also we require $G_{ss'}(\boldsymbol{k}, t = 0^+) = \delta_{s,-s'}$. Finally, there is the question of where to evaluate $\boldsymbol{\Sigma}_1(\omega)$. (Carnevale and Fredericksen 1983*b*). Do we evaluate it at the pole for complex ω or somewhere on the real axis? We chose to evaluate $\boldsymbol{\Sigma}_1(\omega)$ at $\omega = \Omega(\boldsymbol{k})$, with Ω given by the linear dispersion relation. See §3 for further comments. In particular we choose

$$\boldsymbol{\Sigma}_1(\boldsymbol{k}, \omega) = \boldsymbol{\Sigma}_1(\boldsymbol{k}, \Omega), \quad \boldsymbol{\Sigma}_2(\boldsymbol{k}, \omega) = \boldsymbol{\Sigma}_2(\boldsymbol{k}, \Omega). \tag{2.5}$$

The quantities $\boldsymbol{\Sigma}_1$ and $\boldsymbol{\Sigma}_2$ are in general 2×2 matrices with complex components, and so superficially appear to represent 16 real parameters. However, using the constant-ω assumption and the general symmetry conditions

$$\left.\begin{aligned} U^{ss'}(\boldsymbol{k}, \omega) &= [U^{-s,-s'}(-\boldsymbol{k}, -\omega)]^*, \\ U^{ss'}(\boldsymbol{k}, \omega) &= U^{s's}(-\boldsymbol{k}, -\omega), \\ G^{ss'}(\boldsymbol{k}, \omega) &= [G^{-s,-s'}(-\boldsymbol{k}, -\omega)]^* \end{aligned}\right\} \tag{2.6}$$

enables us to reduce these to 7 independent real quantities. We denote

$$\left.\begin{aligned} a(\boldsymbol{k}) &\equiv \Sigma_1^{-+}(\boldsymbol{k}, \Omega) = -[\Sigma_1^{+-}(\boldsymbol{k}, \Omega)]^*, \\ c(\boldsymbol{k}) &\equiv \Sigma_1^{++}(\boldsymbol{k}, \Omega) = -[\Sigma_1^{--}(\boldsymbol{k}, \Omega)]^*, \\ d(\boldsymbol{k}) &\equiv \Sigma_2^{++}(\boldsymbol{k}, \Omega) = (\Sigma_2^{--}(\boldsymbol{k}, \Omega))^*, \\ e(\boldsymbol{k}) &\equiv \Sigma_2^{-+}(\boldsymbol{k}, \Omega) = (\Sigma_2^{+-}(\boldsymbol{k}, \Omega))^*. \end{aligned}\right\} \tag{2.7}$$

The first symmetry condition implies that $e(\boldsymbol{k})$ is real; the other three quantities are in general complex.

By invoking a further assumption we can reduce this set of parameters even further. We proceed as follows: with the above assumption we can write the Green function for this problem as

$$\boldsymbol{G}(\boldsymbol{k}, \omega) = \frac{1}{(\omega - \eta)(\omega - \sigma)} \begin{bmatrix} c^* & \omega + \Omega - a^* \\ \omega - \Omega + a & -c \end{bmatrix}. \tag{2.8}$$

In writing matrices we will use the convention that $s = +$ is represented by the first row (or column). In the expression for $\boldsymbol{G}$

$$\eta \equiv \Omega_r - ia_I, \quad \sigma \equiv -\Omega_r - ia_I, \quad \Omega_r^2 \equiv (\Omega - a_R)^2 - |c|^2. \tag{2.9}$$

Here Ω_r is the renormalized 'frequency'; a_R and a_I represent the real and imaginary parts of a respectively. We note that in the weak-interaction limit $\Omega_r \to \Omega$, but that in this self-consistent calculation Ω_r may be either purely real or purely imaginary depending on the relative values of $\Omega - a_R$ and $|c|$. This will be explored more fully later.

Notice that in this particular case the two poles of the Green function satisfy

$$(\eta + \sigma)^* = -(\eta + \sigma), \quad (\eta\sigma)^* = \eta\sigma. \tag{2.10}$$

This result can be seen directly by comparing with (2.9), but more importantly it can be obtained by applying the symmetry property of $\boldsymbol{G}$ in (2.6) without knowing

the analytical expressions for η and σ. This is useful because the same structure appears when Green functions with more poles are considered. In such cases it is not generally possible to obtain closed-form expressions for the poles.

From the equation for $\boldsymbol{G}$ we can compute the correlation function

$$\boldsymbol{U}(\omega) = \boldsymbol{G}(\omega)\,\boldsymbol{\Sigma}_2\,\boldsymbol{G}^{\mathrm{T}}(-\omega), \tag{2.11}$$

where the superscript T denotes transpose of the matrix. If we denote

$$\boldsymbol{U}(\omega) = [(\omega-\eta)\,(\omega+\eta)\,(\omega-\sigma)\,(\omega+\sigma)]\,\boldsymbol{O}(\omega) \tag{2.12}$$

then $\boldsymbol{O}(\omega)$ has no poles.

Now we are ready to impose 'experimental' constraints on our expressions. The function

$$\boldsymbol{U}(\boldsymbol{k}, t) = \int \mathrm{d}\omega\, \mathrm{e}^{\mathrm{i}\omega t}\,\boldsymbol{U}(\boldsymbol{k}, \omega) \tag{2.13}$$

gives the two-time correlation of the internal-wave amplitudes and is given experimentally by the Garrett–Munk spectra GM72 and GM75 (Garrett & Munk 1972, 1975) and GM76 (Cairns & Williams 1976). We used GM76 in these calculations:

$$\left.\begin{aligned}
U^{ss'}(t=0) &= U(k_{\mathrm{h}}, k_{\mathrm{v}})\,\delta_{s,-s'},\\
U(k_{\mathrm{h}}, k_{\mathrm{v}}) &= E(k_{\mathrm{h}}, \omega)\frac{\partial\omega}{\partial k_{\mathrm{v}}},\\
E(k_{\mathrm{h}}, \omega) &= \frac{E_0}{2\pi}\frac{B(\omega)\,\kappa_*(\omega)}{(k_*(\omega)+k_{\mathrm{h}})^2}\\
B(\omega) &= \frac{2}{\pi}\frac{f}{\omega}\frac{1}{(\omega^2-f^2)^{\frac{1}{2}}}\\
k_*(\omega) &= 6b(\omega^2-f^2)^{\frac{1}{2}},\\
E_0 &= 30\ \mathrm{cm^2/s^2},\\
N_0 &= 5.2\times10^{-3}\ \mathrm{s^{-1}},\\
b &= 4.6\times10^{-3}\ \mathrm{s\ cm^{-1}},\\
f &= 7.3\times10^{-5}\ \mathrm{s^{-1}}.
\end{aligned}\right\} \tag{2.14}$$

We take this as an additional constraint on the equations, although it is probably only true for the large-scale waves. Sufficiently good experimental measurements could provide the $s = s'$ component.

$$d = -\mathrm{i}c(e/a_{\mathrm{I}}) = e/2a_{\mathrm{I}}; \tag{2.15}$$

see (2.7) for the definitions of c, d and e. The last expression is the same one obtained in the WIA. We see that $\boldsymbol{\Sigma}_2$ is completely determined by $\boldsymbol{\Sigma}_1$ and the Garrett–Munk spectrum. This leaves us with only four independent real quantities to compute. The expressions for $\boldsymbol{O}$ under this approach are also greatly simplified:

$$\boldsymbol{O} = \begin{bmatrix} 2a_{\mathrm{I}}\boldsymbol{U} & \dfrac{\mathrm{i}c^*}{a_{\mathrm{I}}}(\omega^2+\eta\sigma) & (\omega+\Omega-a_{\mathrm{R}})^2+a_{\mathrm{I}}^2-|c|^2 \\ (\omega-\Omega+a_{\mathrm{R}})^2+a_{\mathrm{I}}^2-|c|^2 & \dfrac{-\mathrm{i}c}{a_{\mathrm{I}}}(\omega^2+\eta\sigma) & \end{bmatrix}. \tag{2.16}$$

The great benefit of this approach is that we now need only iterate one of the two DIA equations (the equation giving $\boldsymbol{\Sigma}_1$). As a matter of fact if one reviews the steps

taken to derive the final expression for $\boldsymbol{G}$ and $\boldsymbol{U}$ it is not difficult to see that this is generally true whenever $\boldsymbol{\Sigma}_2$ is chosen to be constant, regardless of the functional dependence of $\boldsymbol{\Sigma}_1$ on ω. After the $\boldsymbol{\Sigma}_1$ equation has been solved self-consistently the value of e may be computed from the $\boldsymbol{\Sigma}_2$ equation to determine how close the ratio $e/2a_{\mathrm{I}}$ is to the Garrett–Munk spectrum. If we use the equations in §2 and impose (2.14) and (2.16), it is easy to derive the following balance equation:

$$\frac{F_0(\boldsymbol{k})}{U(\boldsymbol{k})} - 2\nu_0(\boldsymbol{k}) = 2\ \mathrm{Im}\ \Sigma_1^{+-}(\boldsymbol{k}) - \frac{\Sigma_2^{+-}(\boldsymbol{k})}{U(\boldsymbol{k})}. \tag{2.17}$$

If there is no forcing or dissipation on mode k due to non-internal-wave sources, the left-hand side is zero. In this case if the right-hand side is non-zero one would infer some inconsistency. One possibility is that the Garrett–Munk $U(\boldsymbol{k})$ is not correct. A second possibility is that there is either an effective F_0 present or an effective ν_0, i.e. mode $\boldsymbol{k}$ might be driven or damped by direct coupling to the external environment. And of course the theoretical framework and model may be invalid. If the right-hand side is positive then energy is being fed into mode $\boldsymbol{k}$ externally, and if it is negative then energy is being removed.

3. Physical significance of the parameters

Before we display our numerical results for the parameters $\boldsymbol{\Sigma}_1$ and $\boldsymbol{\Sigma}_2$ we would first like to discuss the meaning of the parameters introduced in §2. To do this we recall that the nonlinear evolution equation (2.4) may be equivalently written as a set of effective linear evolution equations, which for the constant-$\boldsymbol{\Sigma}$ case in this paper are

$$\left.\begin{aligned} \dot{A}^+(\boldsymbol{k},t) + (\nu_0 + \mathrm{i}\Omega^* - \mathrm{i}a)\, A^+(\boldsymbol{k},t) + \mathrm{i}c^* A^-(\boldsymbol{k},t) &= f^+(\boldsymbol{k},t), \\ \dot{A}^-(\boldsymbol{k},t) + (\nu_0 - \mathrm{i}\Omega + \mathrm{i}a^*)\, A^-(\boldsymbol{k},t) - \mathrm{i}cA^+(\boldsymbol{k},t) &= f^-(\boldsymbol{k},t). \end{aligned}\right\} \tag{3.1}$$

The functions f^+ and f^- give the effective driving of the waves due to all other modes. The parameter ν_0 is a free parameter that may be used to inject additional information about the decay of internal waves due to interaction with external systems. In all numerical work we always set $\nu_0 = 0$.

The parameter a represents two physical quantities. The imaginary part of a represents an additional effective damping of the internal-wave mode due to losses to other internal-wave modes. The real part of a gives the frequency shift of the wave. The parameter c represents a coupling between + and − travelling waves. See also Holloway (1979).

The pair of first-order equations for the amplitudes may be written as a pair of second-order equations involving only one type of amplitude each. If we ignore the f, then for either A^+ or A^- we have

$$A(\boldsymbol{k},t) + 2(\nu_0 + a_{\mathrm{I}})\, \dot{A}(\boldsymbol{k},t) + [(\Omega - a_{\mathrm{R}})^2 + (\nu_{0+} a_{\mathrm{I}})^2 - |c|^2]\, A(\boldsymbol{k},t) = 0. \tag{3.2}$$

The solution has a time dependence

$$A^{\pm} \sim \exp\{-(\nu_0 + a_{\mathrm{I}})\, t + [|c|^2 - (\Omega - a_{\mathrm{R}})^2\, t]^{\frac{1}{2}}\}. \tag{3.3}$$

If $|c|^2 > (\Omega - a_{\mathrm{R}})^2$ then we refer to the mode as overdamped. In the underdamped case the damping is given by

$$\nu = \nu_0 + a_{\mathrm{I}}. \tag{3.4}$$

In the overdamped case the damping is

$$\nu = \nu_0 + \alpha_{\mathrm{I}} \pm |\Omega_{\mathrm{r}}|. \tag{3.5}$$

We will define

$$\alpha_S = a_I + |\Omega_r|, \quad \alpha_L = a_I - |\Omega_r|. \tag{3.6}$$

In the overdamped region we define

$$A^+ \sim e^{-\alpha_S t} \quad \text{and} \quad A^- \sim e^{-\alpha_L t}. \tag{3.7}$$

A spike disturbance in the equilibrium spectrum will contain both a short-lived and a long-lived component. We will see from the results of the numerical calculations that it is α_L that measures the lifetime of a disturbance for a large part of the internal-wave spectrum.

As the idea of overdamping when applied to waves may seem peculiar we will give our interpretation of the meaning. Perhaps the simplest example is due to Kraichnan (1964). Suppose we have a linear wave field in a medium moving with velocity $\boldsymbol{V}$. The frequency of a $(\boldsymbol{k}, \Omega)$-wave will be

$$\Omega_V = \Omega - \boldsymbol{k} \cdot \boldsymbol{V} \tag{3.8}$$

and time dependencies

$$e^{i\Omega_V t} = e^{i\Omega t} e^{-i\boldsymbol{k} \cdot \boldsymbol{V}}. \tag{3.9}$$

Imagine averaging over an ensemble of velocity $\boldsymbol{V}$:

$$\langle e^{i\Omega_V t} \rangle = e^{i\Omega t} e^{-\frac{1}{2}k^2 t^2 \langle V^2 \rangle}. \tag{3.10}$$

For large enough $\langle V^2 \rangle$ this will represent a strong damping, although not an overdamping. The relevance of this to internal waves is easily seen when we consider the effect of the large-scale waves on the small-scale waves. It has some of the elements of a random velocity field, but it also has the effect of changing the magnitudes of $\boldsymbol{k}$ and Ω as well. The small-scale wave may remain wavelike, but its wave vector changes under the influence of the background field.

If the frequency is also changed in a random way then we have to average over Ω as well. If Ω is a Gaussian random variable with zero mean, then the average

$$\langle e^{i\Omega t} \rangle \sim e^{-\frac{1}{2}\Omega^2 t^2},$$

and we have complete overdamping. The calculations of Henyey & Pomphrey (1983) of small-scale wave packets in a large-scale field show a random behaviour in which the frequency of the wave packet undergoes rapid fluctuations. Our choice of fixed wave vectors $\boldsymbol{k}$ to describe the wave is very awkward in the presence of strong advection and forcing. And of course both our approximation to the DIA and the DIA itself are suspect in this situation.

4. Numerical results

In figure 1 we show a contour plot of $\log |c/(\Omega - \alpha_R)|$ versus $\log m$ on the horizontal axis and $\log \Omega$ on the vertical axis. Here m refers to the vertical wavenumber. The line of critical damping has the value zero; everything to the left of this line is in the underdamped regime, while everything to the right is in the overdamped regime. Certainly the overdamped region is not describable by weak-interaction theory. It is instructive to compare this plot with figure 2, a plot of $\log (a_I(\mathrm{WI})/\Omega)$ for the weak-interaction (WI) case using the same wave vector cutoffs for both. Recall that, for WIA to be valid, one requirement is that the damping timescale must be long compared with the intrinsic frequency; that is, $a_I \ll \Omega$. Notice that the self-consistent overdamped region covers the entire $a_I/\Omega > 1$ region and overlaps the $a_I/\Omega < 1$

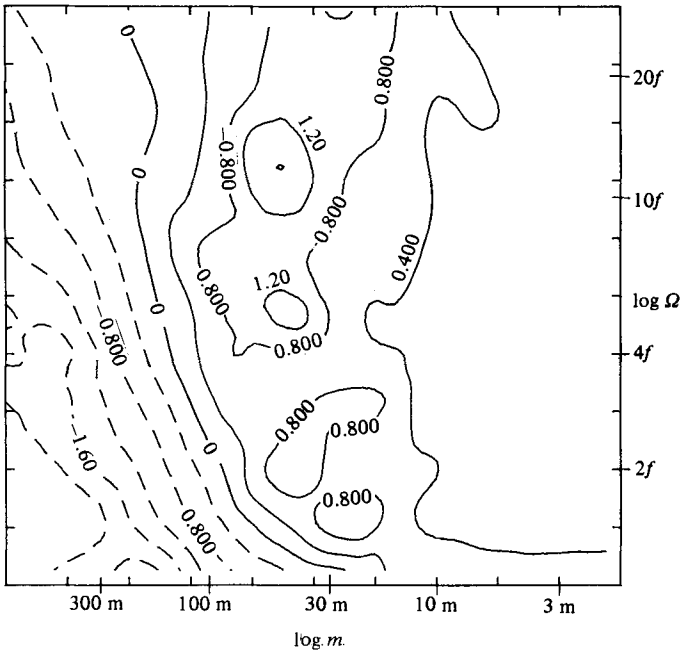

FIGURE 1. Contour plot of $\log |c/(\Omega - a_R)|$ *vs* $\log m$ on the horizontal axis and $\log \Omega$ on the vertical axis. The contour interval is 0.4. The zero line corresponds to critical damping. All modes to be left on this line are underdamped; all lines to the right are overdamped.

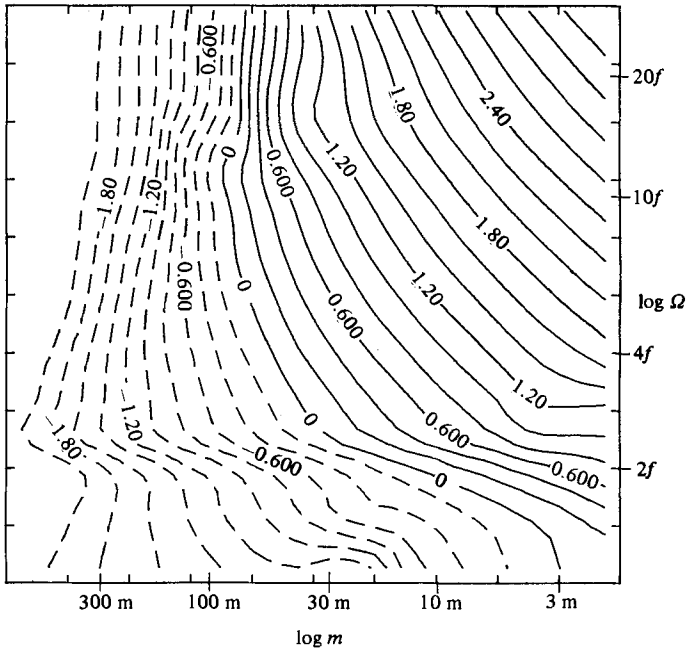

FIGURE 2. Contour plot of $\log a_I(\mathrm{WI})/\Omega$ *vs* $\log m$ on the horizontal axis and $\log \Omega$ on the vertical axis. The contour interval is 0.2. Dashed contours indicate lines with negative values. The horizontal axis is marked off in equivalent vertical wavelengths (in metres) and the vertical axis is marked off in units of the Coriolis frequency.

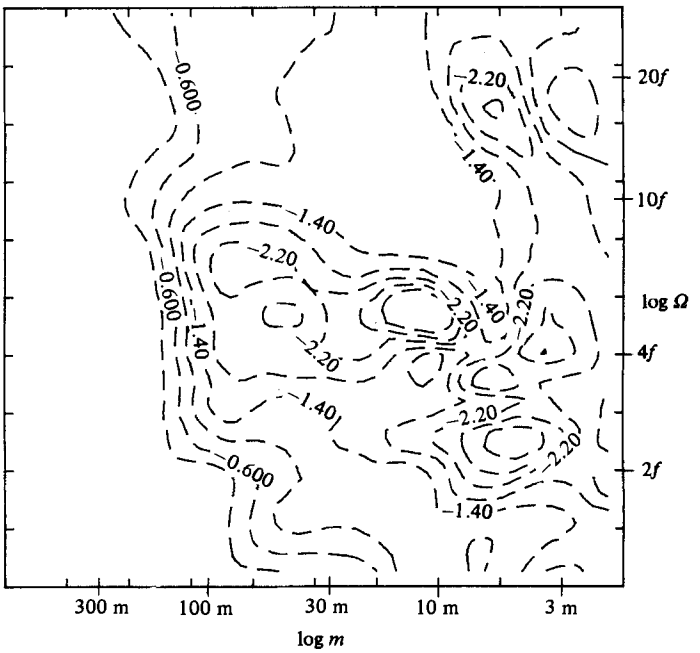

FIGURE 3. Contour plot of $\log|\alpha_L/\alpha_S|$ *vs* $\log m$ on the horizontal axis and $\log\Omega$ on the vertical axis. The contour interval is 0.4.

region, so that the overdamping takes over just in the region where the old weak interaction calculation is known to be invalid. What is interesting is the extent to which the self-consistent (SC) calculaton reduces the rates in the large-m, large-Ω region. Of course we do expect the SC calculation to reduce the damping rates in this region, for reasons described below, but the way that this reduction comes about is rather unexpected. Recall that the rate of decay of a spike disturbance introduced into the steady-state ocean is given by α_L and α_S in the SC calculation (see (36)). If we plot $\log|\alpha_L/\alpha_S|$ in figure 3 we see that in essentially the entire overdamped region $\alpha_L \ll \alpha_S$, which implies that $\alpha_I(\mathrm{SC}) \approx |\Omega_R|$. This means that the decay rates are much smaller than one would expect by examining the scale of a_I. Unfortunately the same device that causes the damping rates to be so greatly diminished also makes it more difficult to obtain accurate numbers in the large-m region. A small change in the parameters (a, c) in this region can cause a disproportionately large change in α_L (though not in α_S). Since it is (a, c) that are computed in each iteration, factors such as the integration accuracy make it difficult to control such changes after a certain limit is reached. We have solved the equations by an iterative scheme. After many iterations the results do not change much, but the cancellations and inaccuracies in the integration scheme lead to some changes from iteration to iteration. In the next two figures we compare the α_I from two successive iterations. Figure 4 is a plot of the percent deviation of the input values of a_I compared to the output values of a_I.

$$\Delta(a_I) \equiv 100\left|\frac{\alpha_I(\mathrm{in})-\alpha_I(\mathrm{out})}{\alpha_I(\mathrm{in})+\alpha_I(\mathrm{out})}\right|. \tag{4.1}$$

In a perfect calculation, of course, these numbers would be identical. We see in fact that in most of the region of interest we have convergence to whtin a few percent,

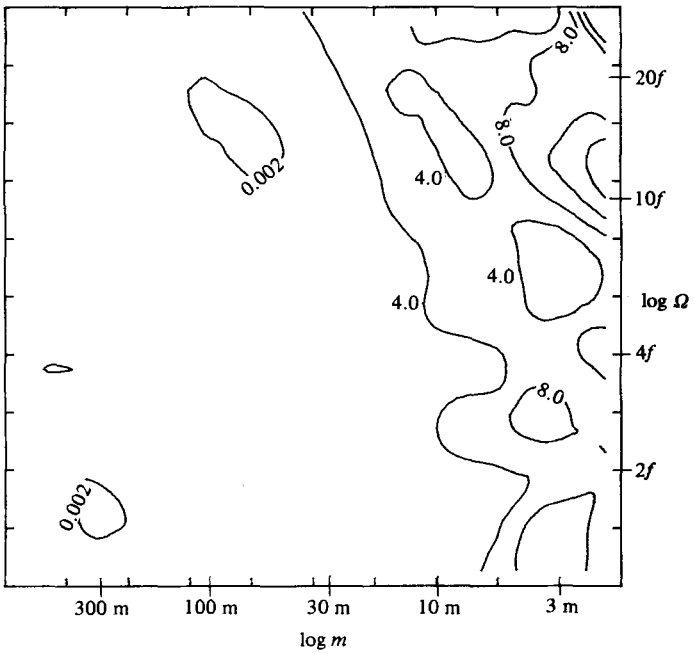

FIGURE 4. Contour plot of $\Delta(a_I)$, the percentage deviation of the input value of α_I compared with the output value, *vs* $\log m$ on the horizontal axis and $\log \Omega$ on the vertical axis.

and it is only for very large values of m that we reach values of 8–10 %. However, if we compare this with figure 5, which is a plot of

$$\log \Delta(\alpha_L) \equiv \log 100 \left| \frac{\alpha_L(\text{in}) - \alpha_L(\text{out})}{\alpha_L(\text{in}) + \alpha_L(\text{out})} \right|, \tag{4.2}$$

we see that the error increases in α_L more quickly than it does in a_I. The contours labelled 1.5 and 2.0 correspond to a 30 % and a 100 % error respectively. In the large-m region this means that we only know α_L within a factor of 2 or so. We hasten to point out that this does not alter our conclusions about the dramatic effects of the SC calculation. First of all the fact that the values of (a, c) for a given mode do not depend on the behaviour of modes with even moderately greater values of (m, Ω) means that the computed values in most of the space are not affected by the uncertainty in the large-m extreme. Second, we will see shortly that compared to the WIA the rates for the SC case in the large-m region are reduced by orders of magnitude, and so even a factor of 2 uncertainty does not eliminate the qualitatively new behaviour.

Referring back to (3.7), we see that $\alpha_L \ll \alpha_S$ implies that, for example,

$$A^-(k, t) \sim e^{-\alpha_L t}, \tag{4.3}$$

so that we may ignore α_S and consider only α_L in determining the long-time behaviour of G. For this reason we plot $\log(\alpha_L/\Omega)$ in figure 6 with the understanding that $\alpha_L = \alpha_I$ in the underdamped regime. It is clear that these rates are very much different from those calculated using the WIA. The rates for most of the spectrum now satisfy $\alpha_L/\Omega \ll (2\pi)^{-1}$, but there still exists a substantial region for which $\alpha_L/\Omega > 1$, mostly in modes with high frequencies. We explicitly compare the WIA decay rates with SC rates in figure 7, where we plot $\log(\alpha_L/a_I(\text{WI}))$. For small m and small Ω both

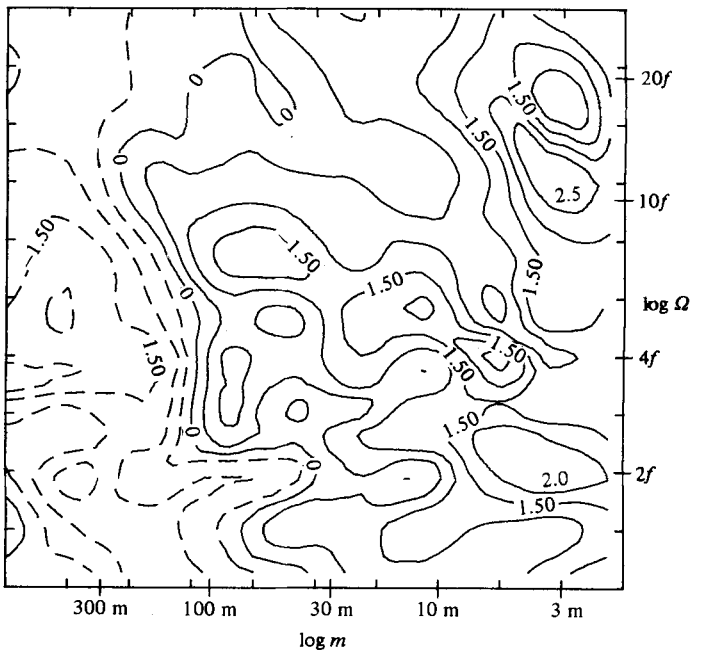

FIGURE 5. Contour lot of $\log \Delta(\alpha_L)$, the logarithm of the percentage deviation of the input value of α_L compared with the output value, *vs* $\log m$ on the horizontal axis and $\log m$ on the vertical axis. The contour interval is 0.5.

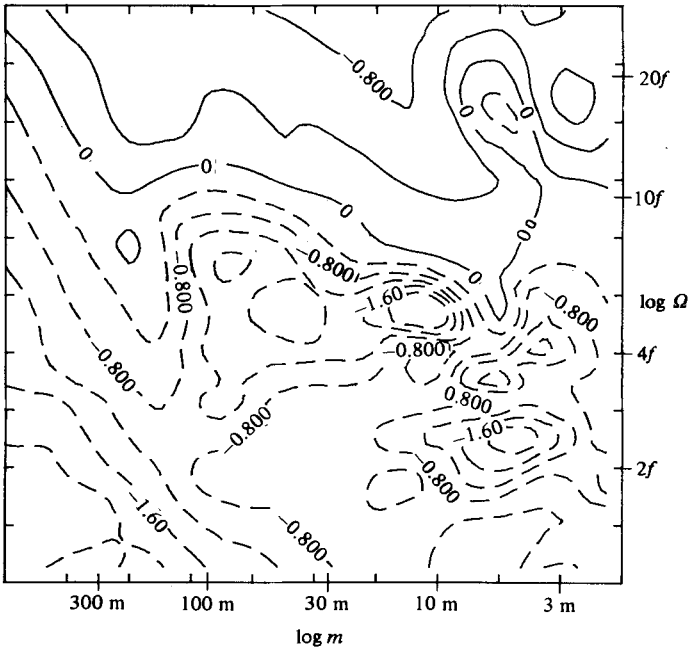

FIGURE 6. Contour plot of $\log|\alpha_L/\Omega|$*vs* $\log m$ on the horizontal axis and $\log \Omega$ on the vertical axis. The contour interval is 0.4.

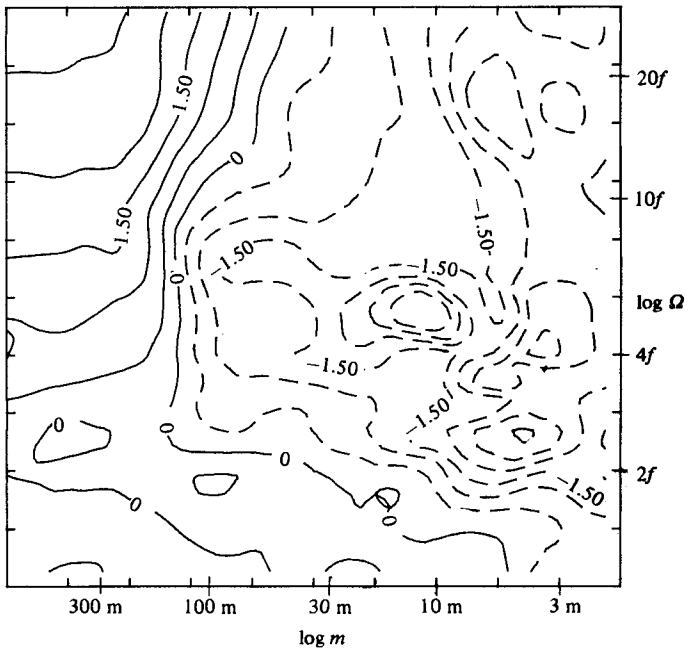

FIGURE 7. Contour plot of $\log|\alpha_L/\alpha_I(\mathrm{WI})|$ *vs* $\log m$ on the horizontal axis and $\log\Omega$ on the vertical axis. The contour interval is 0.5.

calculations give roughly the same results. For moderate-to-large m we see substantially reduced rates for G. Notice though that in the small-m, large-Ω region the SC calculation actually increases rates by a great deal.

The change in rates for moderate-to-large-m region is easy to understand if one remembers that McComas (1977) and McComas & Bretherton (1977) identified the induced diffusion mechanism to be the dominant energy-transfer mechanism for the WIA in this region. This means that energy diffuses from a given large-wave-vector mode to a nearby mode in wave-vector space by interacting with a third, small-wave-vector mode. Since in the WIA all waves are assumed to have infinite lifetimes, the rate of energy exchange is only governed by the coupling between the modes. However, in the SC calculation the finite lifetime of each mode is built into the calculation. This, and the fact that the decay rates depend on the amplitudes of the interacting modes, implies that the rate at which energy is transferred between modes decreases as the waves decay. Therefore we would expect the lifetimes of the modes in this region to be increased.

We would now like to consider another measure of the consistency of the calculation. Recall that we have found a correspondence between e and a given by (2.16). Given the parameters (a, c) we can now compute the ratio $e/2a_I U(0)$. In truth the degree to which $e/2a_I U(0) = 1$ depends both on how well GM76 represents an equilibrium spectrum *and* on the reliability of the calculation. It is not possible under the current assumptions to differentiate between these two effects, so it is best to talk about the degree of equilibrium of GM76 under a given approximation. (See also the discussion at the end of §2.) For example, figure 8 shows a plot of $e/2a_I U(0)$ for the WIA. We see that for large frequencies the spectrum appears to be in a high degree of equilibrium, while the lower frequencies are out of equilibrium by 50% or more. In the region where $e/2\alpha_I U(0)$ is less than 1, energy is being fed in. This occurs for

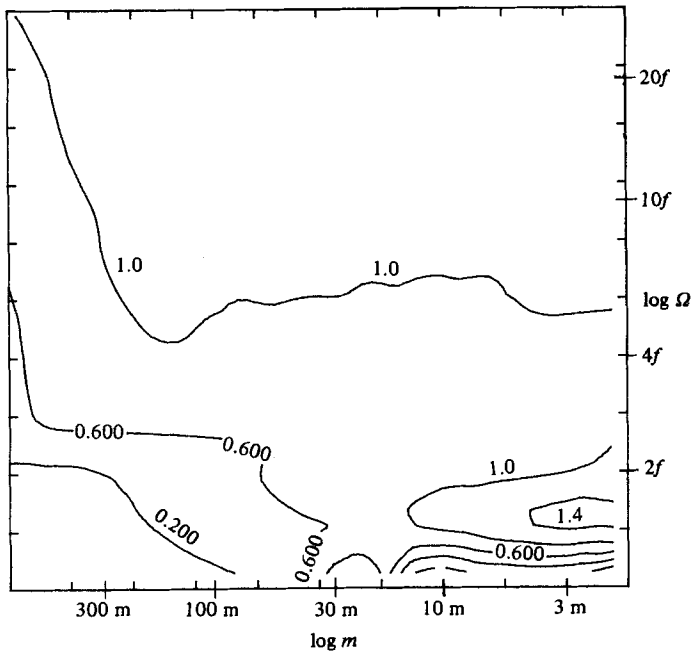

FIGURE 8. Contour plot of $e/2\alpha_1(\mathrm{WI})U(0)$ *vs* $\log m$ on the horizontal axis and $\log \Omega$ on the vertical axis. The contour interval is 0.4.

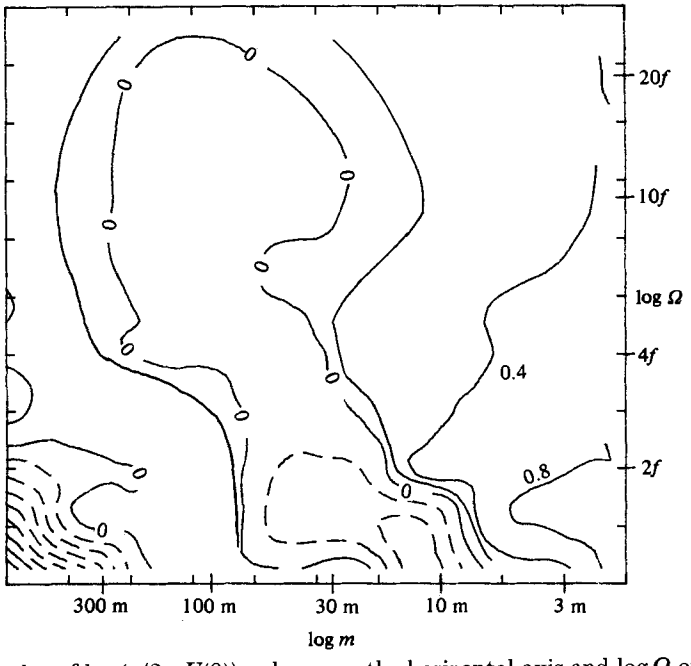

FIGURE 9. Contour plot of $\log(e/2\alpha_1 U(0))$ *vs* $\log m$ on the horizontal axis and $\log \Omega$ on the vertical axis. The contour interval is 0.4. The dashed lines indicate negative values corresponding to energy flowing in.

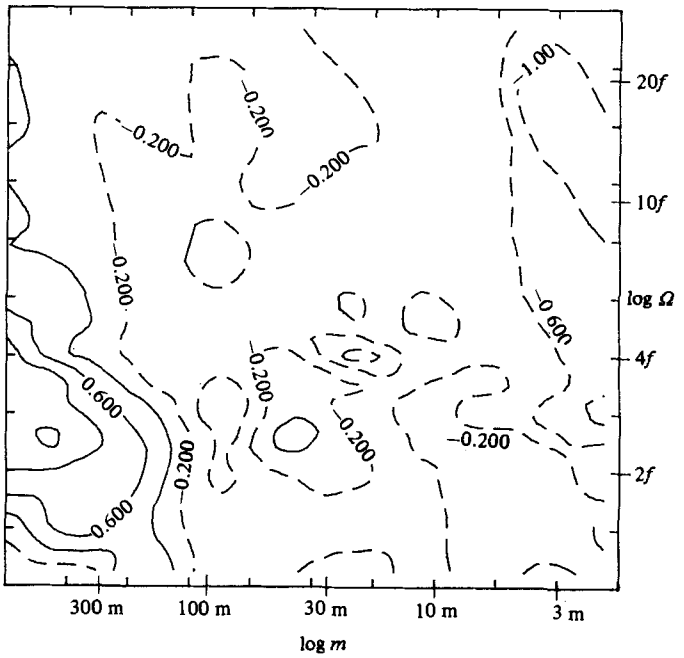

FIGURE 10. Contour plot of $\log|(\mathrm{d}/\mathrm{d}\Omega)\,\hat{\Sigma}_1^{-+}(\Omega)\,\Omega/\Sigma_1^{-+}(\Omega)|$ *vs* $\log m$ on the horizontal axis and $\log\Omega$ on the vertical axis, for the self-consistent calculation. The contour interval is 0.4.

frequencies near f and for large vertical wavelengths. Dissipation occurs for short vertical wavelengths. We compare this with figure 9, which shows $\log(e/2\alpha_{\mathrm{I}}U(0))$ for the SC calculation. We note that the previous discussion concerning the accuracy of α_{L} is relevant here, since a factor of 2 in the high-m region can greatly affect the equilibrium balance. The equilibrium nature of GM76 may be difficult to determine for large-m in this SC calculation. However, in general we obtain a similar kind of deviation of $e/2a_{\mathrm{I}}U(0)$ from 1, the order of 50% or so. There are some important differences between figures 8 and 9. The dissipation rates are higher for larger vertical wavenumber (necessitating the logarithmic contours), and perhaps most important there are indications of some energy dissipation for high-frequency long-vertical-wavelength waves.

Next, we have done another test calculation to determine how much the SC calculation might affect the off-resonant character of Σ_1 and Σ_2. We have calculated the derivative of Σ_1^{-+} at $\omega = \Omega$. In figure 10 we plot

$$\log\left|\frac{\Sigma_1'^{-+}(\Omega)\,\Omega}{\Sigma_1^{-+}(\Omega)}\right|, \tag{4.4}$$

a measure of the rate of deviation of Σ_1^{-+} from its value at $\omega = \Omega$. If this quantity is much greater than 1 then the constant-Σ_1 assumption breaks down. If we compare this with the same quantity calculated for the weak-interaction case, shown in figure 11, we see that the region where the relative deviation exceeds 1 is greatly diminished in the SC case. It should be noted in passing that the very restrictive nature of the weak-interaction calculation (only allowing modes to interact if they satisfy the strict frequency-resonance conditions) allows a new class of interaction to suddenly 'turn on' at $\omega = 2f$, and this accounts for the large derivatives around that frequency.

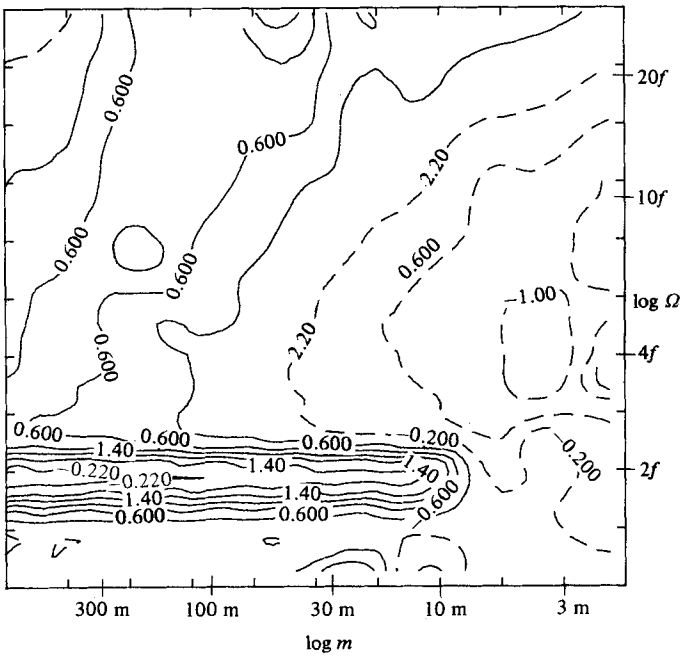

FIGURE 11. Contour plot of $\log|(\mathrm{d}/\mathrm{d}\Omega)\,\dot{\Sigma}_1^{-+}(\Omega)\,\Omega/\Sigma_1^{-+}(\Omega)|$ *vs*/$\log m$ on the horizontal axis and $\log\Omega$ on the vertical axis, for the weak-interaction case. The contour interval is 0.4.

5. Conclusions

In this paper we have described a two-pronged advance in the study of the time behaviour of oceanic internal waves. First, we have applied a formalism which allows for a systematic study of internal-wave interactions. Second we have performed the first self-consistent calculation of oceanic internal-wave parameters. We will first discuss the importance of the formalism.

Olbers (1974, 1976), McComas (1977) and McComas & Bretherton (1977) found high decay rates for internal waves which suggested that the WIA formalism was not appropriate. There have been numerous discussions as to the validity – see McComas & Muller (1981) and Holloway (1980, 1982). Our approach (DeWitt & Wright 1982) provides for a systematic approximation scheme.

The numerical results of this paper indicate the degree to which the earlier numerical calculations were unreliable. In fact we conclude that while that earlier decay rates were basically correct for the small-wave-vector–small-frequency regime, the decay rates for most of the spectrum were much too large. Our calculation indicates that, except for high frequencies, internal waves have a long-lived component that tends to decay relatively slowly. We point out that the fact that *some* region of the spectrum is still predicted to decay quickly provides some support for our procedure. Had all decay rates turned out to be small, we would have been forced into the impossible conclusion that the weak interaction approximation was correct after all. Any future improvements on our calculation cannot change this fact. Further, this argument tends to imply that any future calculation cannot substantially reduce rates in the high-frequency regime, since our numbers there are not much greater than the point where weak-interaction theory becomes valid. This leads us to believe that our rates are fairly representative of reality, or at least represent a rough lower limit to it.

We close by considering how our SC calculation might be improved upon. The most logical next step is to study the effect of non-constant Σ_1 and Σ_2 on the results. This might be done by choosing functional forms for $\Sigma_1(\omega)$ that allow for more than two poles in the Green function. A continued fraction representation of Σ_1 has been tried in other contexts and would probably work well here. The problem with going to a larger number of poles is that it is no longer possible to find analytical expressions for the poles and so some insight might be lost. Further difficulties arise because a continued-fraction representation allows for new poles to appear in G in successive iterations. Since it is not usually possible to keep all of these poles for computational reasons, one must determine a reasonable way to discard some of these poles. Nevertheless choosing some consistent scheme, like keeping the slowest-decaying terms, would make such a calculation an attractive candidate for the next level of calculations.

This research supported in part by ONR under Contract N00014-80-C-0840. The research was performed while both authors were at the University of Illinois, Urbana.

REFERENCES

CAIRNS, T. L. & WILLIAMS, G. O. 1976 Internal wave observations from a midwater float, 2. *J. Geophys. Res.* **81**, 1943–1950.

CARNEVALE, G. F. & FREDERICKSEN, J. S. 1983*a* A statistical dynamical theory of strongly nonlinear internal gravity waves. *Geophys. Astrophys. Fluid Dyn.* **23**, 175–207.

CARNEVALE, G. F. & FREDERICKSEN, J. S. 1983*b* Viscosity renormalization based on direct-interaction closure. *J. Fluid Mech.* **131**, 289–303.

DEWITT, R. J. 1982 Self-consistent effective medium parameters for nonlinear random oceanic internal waves, Ph.D. thesis, Physics Dept, University of Illinois, Urbana.

DEWITT, R. J. & WRIGHT, J. 1983 Self-consistent effective-medium theory of random internal waves. *J. Fluid Mech.* **115**, 283–302.

FREDERICKSEN, J. S., BELL, R. C. 1983 Statistical dynamics of internal gravity waves – turbulence. *Geophys. Astrophys. Fluid Dyn.* **26**, 257–301.

GARRETT, C. J. R. & MUNK, W. H. 1972 Space–time scales of internal waves. *Geophys. Fluid Dyn.* **2**, 225–264.

GARRETT, C. J. R. & MUNK, W. H. 1975 Space–time scales of internal waves. A progress report. *J. Geophys. Res.* **80**, 291–297.

HENYEY, F. S. & POMPHREY, N. 1983 Eikonal description of internal wave interactions, a non-diffusive picture of induced-diffusion. *Dyn. Atmos. Oceans* **7**, 189–220.

HENYEY, F. S., POMPHREY, N. & MEISS, J. D. 1983 Comparison of short-wavelength internal wave transport theories. *La Jolla Inst. Preprint* LJI-R-783-248.

HOLLOWAY, G. 1979 On the spectral evolution of strongly interacting waves. *Geophys. Astrophys. Fluid Dyn.* **11**, 271–287.

HOLLOWAY, G. 1980 Oceanic internal waves are not weak waves. *J. Phys. Oceanogr.* **10**, 906–914.

HOLLOWAY, G. 1982 On interaction time scales of oceanic internal waves. *J. Phys. Oceanogr.* **12**, 293–296.

HOLLOWAY, G. & HENDERSHOTT, M. C. 1977 Stochastic closure for nonlinear Rossby waves. *J. Fluid Mech.* **82**, 747–765.

KRAICHNAN, R. H. 1959 The structure of isotropic turbulence at high Reynolds numbers. *J. Fluid Mech.* **5**, 497–543.

KRAICHNAN, R. H. 1964 Kolmogorov's hypothesis and Eulerian turbulence theory. *Phys. Fluids* **7**, 1723–1734.

MCCOMAS, C. H. 1977 Equilibrium mechanisms within the oceanic internal wave field. *J. Phys. Oceanogr.* **7**, 836.

McComas, C. H. & Bretherton, F. P. 1977 Resonant iteractions of oceanic internal waves. *J. Geophys. Res.* **82**, 1397.

McComas, C. H. & Muller, P. 1981 The dynamic balance of internal waves. *J. Phys. Oceanogr.* **11**, 970–986.

Meiss, J. & Watson, K. M. 1982 Internal-wave interactions in the induced-diffusion approximation. *J. Fluid Mech.* **117**, 315–341.

Meiss, J. D., Pomphrey, N. & Watson, K. M. 1979 *Proc. Natl Acad. Sci. USA* **76**, 2109.

Olbers, D. J. 1974 On the energy balance of small-scale internal waves in the deep sea. *Hamburg Geophys. Einzelschr.* no. 24, *GML Wittenborn Sohnes*, Hamburg.

Olbers, D. J. 1976 Nonlinear energy transfer and the energy balance of the internal wave field in the deep ocean. *J. Fluid Mech.* **74**, 375–399.

Pomphrey, N., Meiss, J. D. & Watson, K. M. 1980 Description of nonlinear internal wave interactions using Langevin methods. *J. Geophys. Res.* **85**, 1085–1094.